Title

Controlling electron beam-induced structure modifications and cation exchange in cadmium sulfide—copper sulfide heterostructured nanorods

Authors

Zheng, Haimei

Sadtler, Bryce

Habenicht, Carsten

et al.

Publication Date

2013-11-01

DOI

10.1016/j.ultramic.2013.05.004

Peer reviewed

Ultramicroscopy 134 (2013) 207–213

Contents lists available at ScienceDirect

Ultramicroscopy

journal homepage: www.elsevier.com/locate/ultramic

Controlling electron beam-induced structure modifications and cation exchange in cadmium sulfide–copper sulfide heterostructured nanorods

Haimei Zheng [a], Bryce Sadtler [b,1], Carsten Habenicht [b], Bert Freitag [c], A. Paul Alivisatos [a,b], Christian Kisielowski [d,e,*]

[a] Materials Sciences Division, Lawrence Berkeley National Laboratory, Berkeley, CA 94720, USA
[b] Department of Chemistry, University of California, Berkeley, CA 94720, USA
[c] FEI Company, P.O. Box 80066, KA 5600 Eindhoven, The Netherlands
[d] National Center for Electron Microcopy, Lawrence Berkeley National Laboratory, Berkeley, CA 94720, USA
[e] Joint Center for Artificial Photosynthesis, Berkeley, CA 94720, USA

ARTICLE INFO

Available online 22 May 2013

Keywords:
Heterostructured nanocrystals
Electron beam irradiation
Exit-wave reconstruction
Aberration corrected TEM
Phase transition

ABSTRACT

The atomic structure and interfaces of CdS/Cu_2S heterostructured nanorods are investigated with the aberration-corrected TEAM 0.5 electron microscope operated at 80 kV and 300 kV applying in-line holography and complementary techniques. Cu_2S exhibits a low-chalcocite structure in pristine CdS/Cu_2S nanorods. Under electron beam irradiation the Cu_2S phase transforms into a high-chalcocite phase while the CdS phase maintains its wurtzite structure. Time-resolved experiments reveal that Cu^{+}–Cd^{2+} cation exchange at the CdS/Cu_2S interfaces is stimulated by the electron beam and proceeds within an undisturbed and coherent sulfur sub-lattice. A variation of the electron beam current provides an efficient way to control and exploit such irreversible solid-state chemical processes that provide unique information about system dynamics at the atomic scale. Specifically, we show that the electron beam-induced copper–cadmium exchange is site specific and anisotropic. A resulting displacement of the CdS/Cu_2S interfaces caused by beam-induced cation interdiffusion equals within a factor of 3–10 previously reported Cu diffusion length measurements in heterostructured CdS/Cu_2S thin film solar cells with an activation energy of 0.96 eV.

1. Introduction

CdS/Cu_2S bi-layer thin films were investigated for solar cell applications between the 1960s and the 1980s because of their favorable band structures and the well-matched absorption spectrum with the solar spectrum [1]. However, engineering the interfaces of CdS/Cu_2S heterojunctions to reduce trap states and to prevent the diffusion of copper from Cu_2S into CdS is a formidable challenge and affects the long-term performance of the solar cell devices [2]. With the advent of new approaches to photovoltaic that incorporate nanostructured light-absorbers, this materials combination has drawn renewed attention [3–7]. Nonetheless, it remains likely that diffusion-mediated alterations occur in heterostructured nanocrystals during device operation even though they can be free of other extended defects. Consequently, it is desirable to better understand the discrepancies and similarities of the transformation and degradation mechanisms in thin films [8] and in nanomaterials [9], which is now possible by applying advanced electron microscopy techniques that recently emerged [10,11].

There are several copper sulfide phases with a chemical composition Cu:S close to 2:1 as pointed out in the Cu–S phase diagram by Potter [12]. At room temperature, Cu_2S exhibits a low-chalcocite structure with an ordered copper lattice embedded in a hexagonal close-packed sulfur sub-lattice. Evans' work [13,14] shows that the crystal structure of low-chalcocite is monoclinic with the space group $P2_1/c$. At 103 °C, bulk Cu_2S crystals transform into a high-chalcocite phase, where copper atoms are rearranged but the hexagonal sulfur sub-lattice is maintained (space group $P6_3/mmc$). This phase transformation temperature is reduced close to room temperature if the Cu_2S nanorods are grown with a diameter of only 4 nm or smaller due to volume and surface contributions to the phase stability [15].

Recently, the phase transformation from a low-chalcocite into a high-chalcocite structure has been observed time-resolved at

* Corresponding author at: National Center for Electron Microcopy, Lawrence Berkeley National Laboratory, Berkeley, CA 94720, USA. Tel.: +1 5104864716.
E-mail address: CFKisielowski@lbl.gov (C. Kisielowski).
[1] Current address: Division of Chemistry and Chemical Engineering, California Institute of Technology, 1200 East California Boulevard, Pasadena, CA 91125, USA.

0304-3991/$ - see front matter © 2013 Elsevier B.V. All rights reserved.
http://dx.doi.org/10.1016/j.ultramic.2013.05.004

atomic resolution [9]. However, it remains challenging to identify the atomic structure of Cu_2S in partially exchanged CdS/Cu_2S nanocrystal heterostructures and to characterize their interfaces because the structural integrity of nanocrystals is commonly compromised by their exposure to the electron beam during observation. In this work, we use lattice imaging with different voltages and dose rates in combination with exit wave reconstruction to study the atomic structure of CdS/Cu_2S nanorods using the TEAM 0.5 microscope. Other TEM techniques are employed to provide complementary information, and they include energy filtered TEM (EFTEM) and electron diffraction from a single nanoparticle at cryogenic temperature. It is the goal of this paper to understand electron beam induced changes to the heterostructured nanorods in order to minimize unwanted sample alterations and to provide an estimate for the Cu^+ and Cd^{2+} exchange across the CdS/Cu_2S interface in a heterostructured nanorod.

2. Experiments

Our CdS/Cu_2S heterostructured nanorods are synthesized by partial cation exchange of Cu^+ and Cd^{2+} within a CdS nanorod in solution [5]. By controlling the reaction conditions, we can grow CdS/Cu_2S binary nanorods of different morphologies and different volume ratios of the two phases. An excess of Cu^+ cations in the reaction solution leads to the full conversion of CdS into Cu_2S. Specifically, CdS/Cu_2S nanorods are grown by adding the precursor solution tetrakis(acetonitrile)copper(I) hexafluorophosphate ($[MeCN]_4Cu(I)PF_6$) in methanol to a stirring solution of CdS nanorods in toluene at room temperature. Ion exchange between Cu^+ and Cd^{2+} converts the CdS into a partially exchanged CdS/Cu_2S heterostructured nanorod or a fully exchanged Cu_2S nanorod by injecting copper atoms and removing cadmium atoms from the rod into the environment. TEM samples are prepared by dropping a solution of nanocrystals on a TEM grid. Ultra-thin carbon films (about 3 nm) on holey carbon supported by copper mesh are used (purchased from Ted Pella, Inc.).

In-line holography has been performed using the TEAM 0.5 microscope, which is an aberration-corrected microscope with 50 pm spatial resolution [10]. It is equipped with a high-brightness Schottky-type field emission gun, a Wien-filter monochromator and can be operated between 20 kV and 300 kV [11,16]. A largest contrast can be achieved by operating at 80 kV [11]. Complex electron exit wave functions of the heterostructured nanorods are reconstructed from through-focus series of up to 35 images during a recording time of about one minute. In this research area W.O. Saxton [17,18] has pioneered early work. Subsequently, Van Dyck et al. have greatly contributed making the focus variation approach a reliable concept that nowadays is most commonly applied [19–22] and further developed. For example, a three-dimensional object reconstruction from one single projection at atomic resolution [23,24] is enabled by in-line holography. In this work, a Gerchberg–Saxton algorithm is utilized for the reconstruction of in-line holograms from focal series of images [25]. The process is implemented in the McTempas software package [26] that is also used for image simulations by multislice calculations. The time dependence of electron beam-induced object changes, which occur during the acquisition of a focus series, is visualized by comparing phase images that are reconstructed from the sequential subsets of images from a single focus series (e.g. reconstruction from images 1–10, 11–20, 21–30).

The electron diffraction studies were conducted at 200 kV with Koehler illumination using a ZEISS Libra 200 FE microscope that is equipped with a field emission gun and an in-column OMEGA energy filter. A cryogenic sample holder is used to record diffraction patterns close to liquid nitrogen temperature. Finally, we acquired energy filtered TEM images (EFTEM) with a 200 kV FEI monochromated F20 UT Tecnai microscope, which is equipped with a field emission gun, a High Angle Annular Dark Field detector (HAADF), and a Gatan Image Filter (GIF). The three-window technique

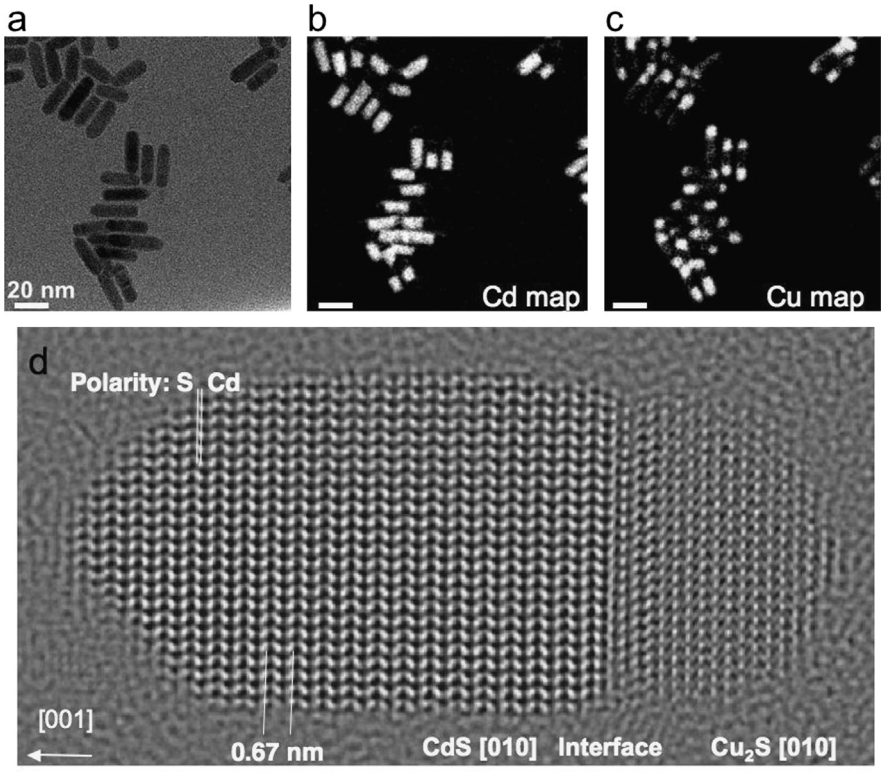

Fig. 1. Images of a CdS/Cu_2S nanorod recorded at 200 kV (EFTEM) and 300 kV (TEAM 0.5). (a) Zero loss image at Scherzer focus. (b) Energy filtered Cd map. (c) Energy filtered copper map. (d) Phase image of a CdS/Cu_2S [010] nanorod showing the CdS/Cu_2S heterojunction interface.

was employed to produce elemental maps of cadmium and copper from CdS/Cu_2S nanorods [27]. They are calculated using two pre-edge images and a post-edge image at 354 eV, 384 eV and 454 eV for the cadmium $M_{4,5}$ edge and 866 eV, 905 eV and 961 eV for the copper L_3 edge, respectively. An energy slit width of 30 eV is used.

3. Results and discussions

3.1. Atomic structure and interfaces in CdS/Cu_2S nanorods

The structure of a single CdS/Cu_2S nanorod and the cadmium or copper element distribution within such rods are displayed in Fig. 1. The elemental maps of Fig. 1b and c show that the cation exchange reaction produces discrete segments of Cu_2S, which predominantly nucleate at the ends of the CdS nanorods (Fig. 1a). Further, the phase of the electron exit wave function in Fig. 1d provides detailed information concerning the CdS/Cu_2S interface: All heterointerfaces are strictly coherent and the most common orientation relationships are $\{001\}_{CdS}\|\{001\}_{Cu_2S}$ and $\{101\}_{CdS}\|\{101\}_{Cu_2S}$ with the [010] directions being aligned and forming the common pole axis in Fig. 1d. Image simulations confirm that CdS crystallizes in the space group $P6_3mc$ with lattice parameters of $a=0.4134$ nm and $c=0.671$ nm while Cu_2S has the space group $P6_3/mmc$. The copper lattice sites are, however, only partly occupied and occupation factors are as low as 0.2–0.6. Therefore, one expects that the unoccupied copper lattice sites will ease copper migration and will significantly contribute to any interdiffusion process. Closer inspection of the image contrast, C, in Fig. 1d allows for a differentiation between sulfur, cadmium, and copper columns by visual inspection in surface proximity. Multislice calculations show (see Fig. 7) that the phase contrast from single atoms increases with their atomic number by approximately $Z^{2/3}$ ($Z_{Cd}=48$, $Z_{Cu}=29$, $Z_S=16$) since there is the general trend that scattering factors increase with Z. Therefore, one expects a contrast sequence $C_{Cd} > C_{Cu} > C_S$. For partly occupied atom columns, however, this sequence can change to $C_{Cd} > C_S > C_{Cu}$ in thin samples. Indeed, image simulations directly verify that partly occupied copper columns must appear darker than sulfur columns as we observe throughout this paper. Fig. 1a shows that the observed nanorods are commonly "pencil shaped". The identification of copper and cadmium columns in Fig. 1d directly links the crystal polarity to the "pencil shape" of the nanorod. Finally, one expects electron beam-induced structure alterations to be present because the space group $P6_3/mmc$ of Cu_2S is a high-temperature phase, which should not occur at room temperature in thermal equilibrium [9].

Fig. 2 shows another phase image of a CdS/Cu_2S heterostructured nanorod that is analyzed in great detail. The smaller volume fraction of the cadmium sulfide phase in the CdS/Cu_2S nanorod of Fig. 2d indicates that the Cu^+–Cd^{2+} cation exchange has advanced to a late stage during synthesis. The phase image was reconstructed from a through-focus series of 35 images at 300 kV. The sections a and b of Fig. 2 show enlarged regions of CdS and Cu_2S phases where the chemical content in the atom columns was determined by comparison with simulations. It is noticed that in a Cd–S dumbbell the sulfur atom is directed toward the sharp end of the rod in [001] direction while the cadmium atom points toward its flat end. This polarity of the CdS nanorod supports a previously proposed growth model [28–30], which links different growth rates of the polar $\pm$ (001) planes to the "pencil shape" of the nanorods. Additionally, there is a pronounced Moire pattern formed in a region of overlapping CdS and Cu_2S lattices on a (110) plane in Fig. 2d. The resolution in the image is 0.1 nm because of a chosen sampling rate of 0.03 nm/pixel, which reflects a compromise between resolution and electron dose. Magnified views of the (101) interface close to the sharp end of the rod and the (001) interface closer to its flat bottom are of interest and shown magnified in Fig. 3. We used straight lines to frame the interface region that is narrower for the (101) interface (Fig. 3a) than for the (001) interface (Fig. 3b). In these areas elliptical marks enclose atom columns where the Cu^+–Cd^{2+} cation exchange took

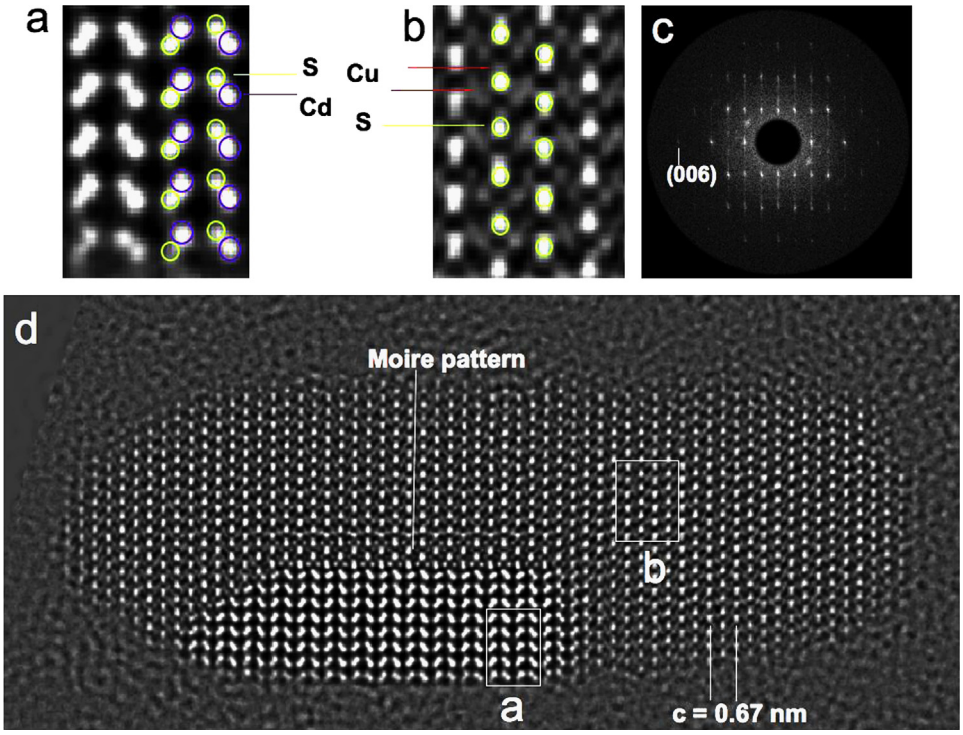

Fig. 2. Phase image of a CdS/Cu_2S nanorod at 300 kV. The zone axis of [010] is identified. (a) CdS with the occupation of columns with Cd and S atoms indicated. (b) High-chalcocite Cu_2S with the occupation of columns with copper and sulfur atoms indicated (c) Fourier transform of a single image with the (006) reflection at 1.1 Å indicated. (d) Phase image of a Cu_2S–CdS heterostructured nanorod. The regions shown in (a) and (b) are marked with white boxes in (d).

place, which is recognized by contrast changes that cannot be understood by modeling stoichiometric crystals that are attached to each other in an abrupt fashion. The different width of these interfaces highlight that the Cu^{+}–Cd^{2+} exchange is anisotropic along different crystallographic directions and yields diffusion distances that can vary by a factor of 2–3. We further notice that the copper/cadmium exchange occurs within a rigid frame of the sulfur sub-lattice.

3.2. Electron beam-induced interface migration

Due to the high mobility of Cu^{+} ions, interface roughening by cation exchange is potentially a degradation mechanism that can limit the deployment of CdS/Cu_2S nanorods in solar cells. Next we show that the migration of the CdS/Cu_2S interface under electron beam irradiation is a quantitative measure for its stability. For this purpose, we have reconstructed the phase image of Fig. 2d from three image subsets of the series. Fig. 4a shows this reconstruction from images 1–10, Fig. 4b utilized images 11–20 and in Fig. 4c we reconstruct the phase of the exit wave function from images 21–30. In this process we gain time resolution at cost of a degrading signal-to-noise ratio. The difference in beam exposure of the later two sets compared to the first one is an additional 15 s and 30 s of exposure time, which corresponds to an additional electron dose of 3.0×10^{4} e/Å^2 and 6.0×10^{4} e/Å^2, respectively. A comparison of the three phase images allows tracking the position of interfaces as the Cu_2S phase moves into CdS phase within the nanorod during image acquisition. It is seen from the visual aids (solid lines) in Fig. 4 that the (101) interface moves about 0.3 nm and the (001) interface ~1.1 nm during the 45 s of recording time. From these two values one calculates an averaged diffusion length of 0.9 nm for 1 min of exposure with a dose rate of 2.0×10^{3} e/Å^2/s at 300 kV. As a result, the beam-stimulated migration of the interface, which is driven by copper/cadmium exchange, can be compared with published copper diffusion data as will be discussed next.

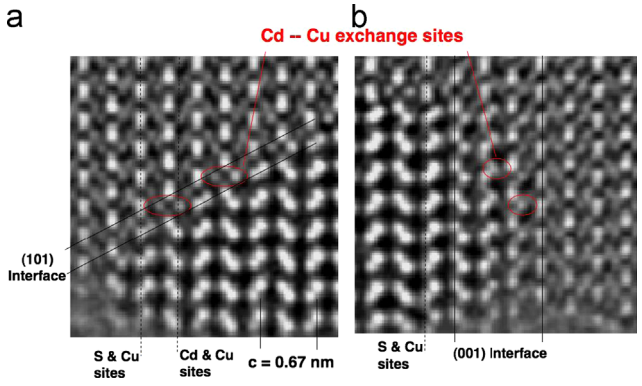

Fig. 3. Sections of phase image of a CdS/Cu_2S nanorod, which show the (101) interface in (a) and the (001) interface in (b). Some copper/cadmium exchange sites are marked. Solid black lines mark the interface regions. The interface structure is coherent. Dashed lines highlight the chemical composition in selected columns of projected atom columns.

3.3. Minimizing electron beam–sample interactions

Considering the result that the electron beam stimulates interdiffusion in the heterostructured nanorod together with our previous finding [9] that a phase transformation of a low-chalcocite to a high-chalcocite structure can be stimulated in Cu_2S by exposure to the electron beam, we test several approaches to minimize beam–sample interactions including a reduction the electron dose, lowering the acceleration voltage and cooling the sample.

First, we find that decreasing the acceleration voltage from 300 kV to 80 kV alone does not retard the phase transition in Cu_2S. However, since the electron-to-photon conversion efficiency of the

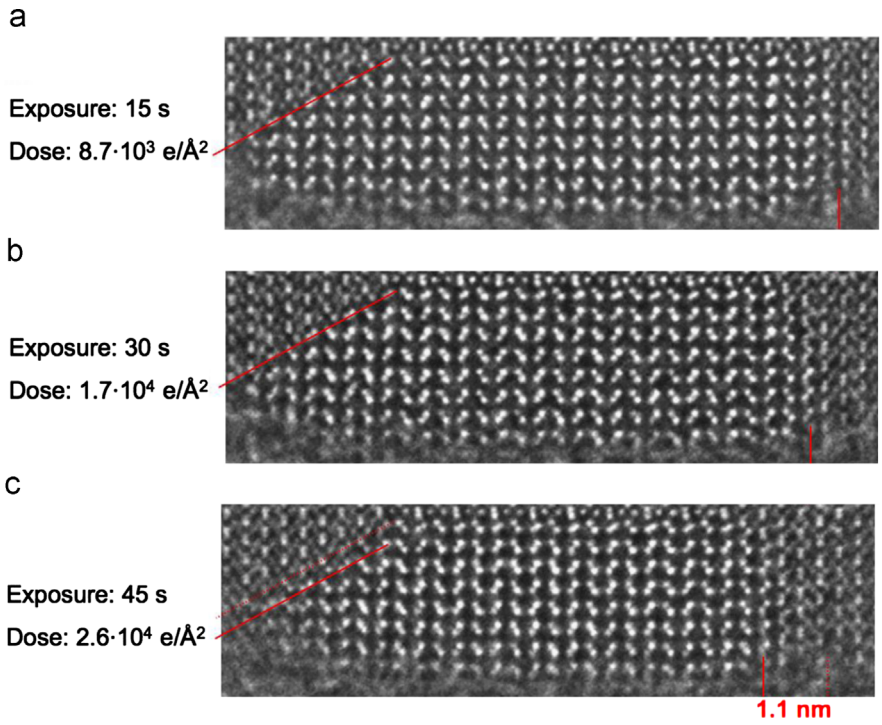

Fig. 4. Phase images of a CdS/Cu_2S nanorod reconstructed from three subsets of images from a focus series used to reconstruct the Fig. 2d. Solid lines mark interface locations. (a) Phase image reconstructed using (1–10) images from the focus series. (b) Phase image reconstructed using (11–20) images from the focus series. (c) Phase image reconstructed using (21–30) images from the focus series. The red lines mark the CdS/Cu_2S interface. For comparison in (c), the initial location of the interface is marked with a dashed red line. (For interpretation of the references to color in this figure legend, the reader is referred to the web version of this article.)

charge coupled device (CCD camera) is higher at 80 kV than at 300 kV (electron/photon conversion factors are ~10 at 80 kV, ~2.5 at 300 kV) and since the scattering contrast increases upon voltage reduction, we operate the TEAM 0.5 at 80 kV with a smaller current density of 800 e/Å^2/s. In such conditions, the atomic structure of the low-chalcocite Cu_2S phase is indeed maintained long enough to record a focus series of 10 images. They were reconstructed to show the phase image in Fig. 5a. The nano-diffraction patterns, which are calculated from the Fourier transform of the electron exit wave functions before and after stimulating the phase transformation, are shown in Fig. 5b and c together with their crystal structures. A distinctly different diffraction pattern of the low and the high-chalcocite phase allows for a unique identification of both phases.

Probing for beam-induced heating effects, we employ a cryo-stage to cool CdS/Cu_2S nanorods close to liquid nitrogen temperature (~80 K). Electron diffraction patterns are collected at 200 kV from a single particle with a dose rate of ~800 e/Å^2/s. Fig. 6a is an image of a CdS/Cu_2S nanorod including the projected condenser aperture that is used for selected area diffraction. The corresponding electron diffraction pattern along the [210] zone axis of the nanorod is shown in Fig. 6b. It highlights the epitaxial relationship of the CdS phase with the high-chalcocite Cu_2S phase that is simulated in Fig. 6c. Obviously, cooling of the sample to liquid nitrogen temperature does not prevent Cu_2S from transforming into a high-chalcocite phase during irradiation, which suggests that dose rates that are commonly used for imaging at atomic resolution overwhelm temperature contributions. Thus, current and voltage reductions are the only feasible options to minimize beam sample interactions, which is why they are currently pursued to enable atomic resolution in beam sensitive materials [11].

4. Discussion and conclusion

The thermodynamic driving force for a cation exchange in a solution originates from the differences of solvation energies for Cu^+ and Cd^{2+} ions [5]. This exchange can also be driven by electron irradiation because it increases the systems' inner energy through phonon excitations, atom displacements or ionization [11]. Currently, the development of in-line holography with variable voltage and dose rate [11] is an emerging strategy to prevent, control and exploit beam–sample interactions. Indeed, it is quite

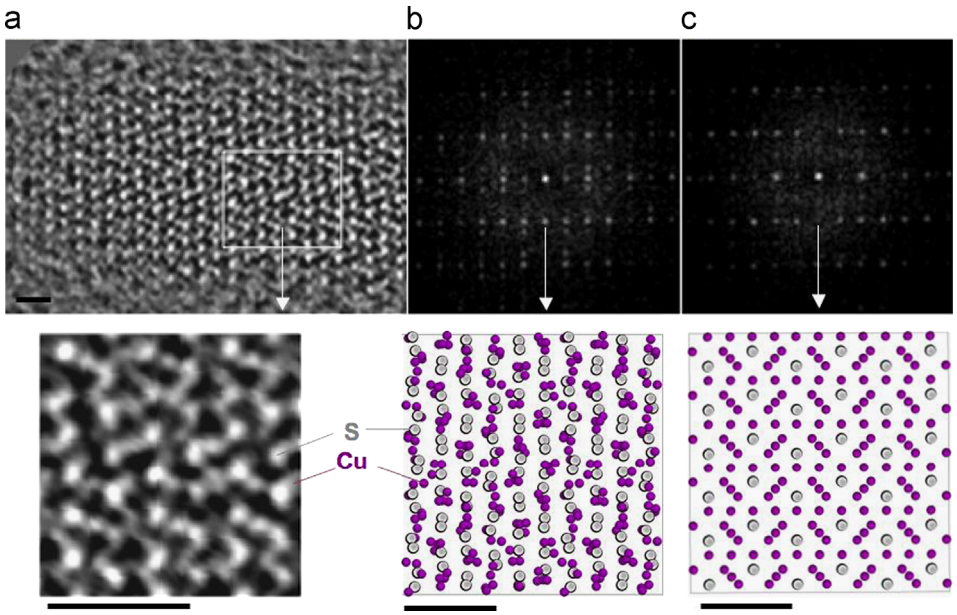

Fig. 5. (a) Reconstructed phase image of a Cu_2S section from a CdS/Cu_2S nanorod recorded at 80 kV. (b) Nano-diffraction pattern (Fourier transform) of (a) showing the low-chalcocite structure of Cu_2S along [010] together with the crystal structure. (c) Nano-diffraction pattern (Fourier transform) showing the high-chalcocite structure of Cu_2S along [010] after extended irradiation together with the crystal structure. The scale bar is 0.7 nm.

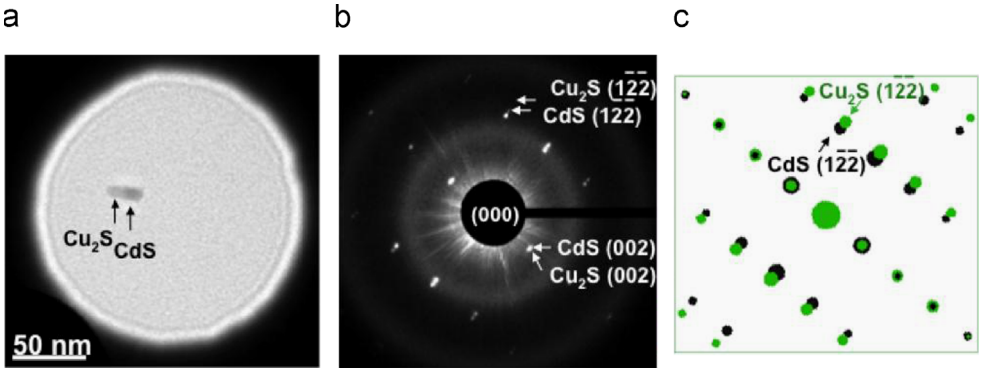

Fig. 6. Bright field image (a) and electron diffraction pattern (b) of a CdS/Cu_2S nanorod recorded at 80 K. (c) Simulated electron diffraction pattern from wurtzite CdS (black) and high chalcocite Cu_2S (green) along the [210] zone axis. (For interpretation of the references to color in this figure legend, the reader is referred to the web version of this article.)

surprising that beam-induced sample excitations do not simply cause unstructured material disintegration. Instead, a view emerges that they commonly stimulate processes that are energetically relevant and provide physically meaningful insight into the dynamic behavior of the investigated material. Here, we strengthen this aspect by comparing the electron beam induced copper/cadmium interdiffusion across and epitaxial CdS/Cu_2S interface with previous measurements of temperature dependent copper diffusion experiments in polycrystalline thin film CdS/Cu_2S solar cells [31]. This comparison is made in Fig. 7a, which depicts our data together with copper diffusion lengths along grain boundaries and in single grains (midgrain) that were calculated from the literature values using activation energies of 0.96 and 0.23 eV. Concerning our data, the Cu_2S phase transition temperature from a low-chalcocite phase to high-chalcocite phase is size dependent and occurs in the chosen nanorods at 337 ± 4 K [9]. Also, it is estimated that a Cu_2S nanorod is heated to ~347.8 K under irradiation with 5000 e/Å^2/s at steady-state [9]. In Fig. 7a we allow for an uncertainty of ± 10 K for this temperature estimation. It is seen that grain boundary diffusion data coincide within a factor of 3–10 with our data and that copper diffusion in single grains exceeds our measured value by a factor of 15–20 at this temperature. Therefore, one recognizes a tendency that copper/cadmium interdiffusion proceeds slower in nanorods than the copper diffusion in thin-film solar cells. This comparison highlights a potential advantage for the use of nanocrystal heterostructures as solar cells: Ion exchange may proceed slower across epitaxial CdS/Cu_2S interfaces in nanorods than copper diffusion in polycrystalline CdS/Cu_2S thin film solar cells at moderate temperatures.

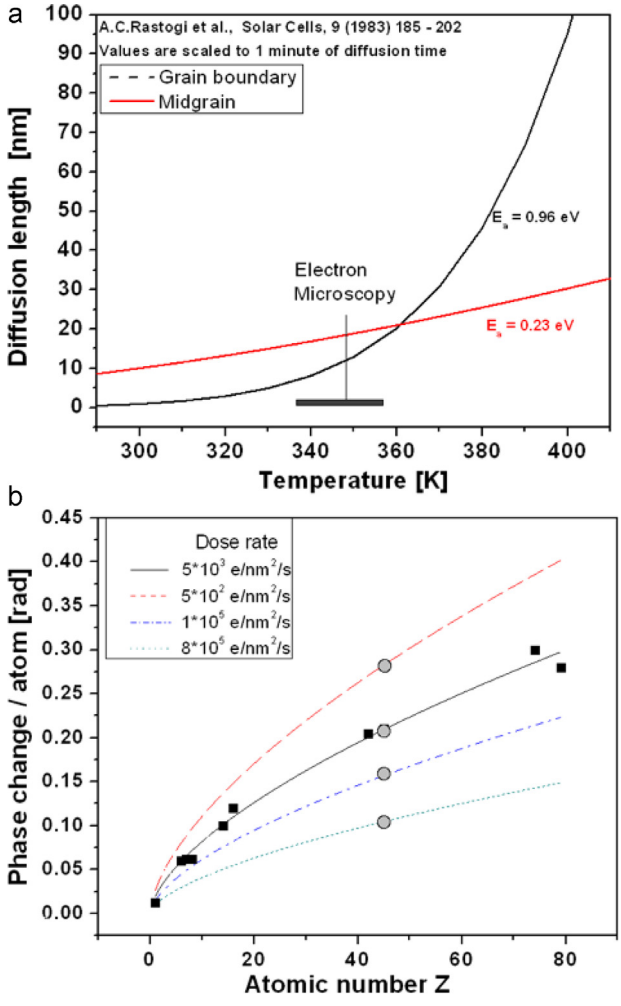

Fig. 7. (a) Temperature dependent diffusion length measurements from [8] are compared with the beam-induced interface migration that is driven by copper/cadmium exchange. The width of the black line represents the error in the temperature measured under the electron beam. (b) Phase contrast dependence on electron dose rate. Calculation (square, lines) and measurement (circles) for single atoms with atomic number *Z*. Data from [32].

One may further consider extracting the number of copper, cadmium and sulfur atoms column-by-column from the phase images that are shown in this paper in order to determine the local chemical composition and diffusion gradients from the complex exit wave function. Such measurements are possible but beyond the scope of this paper because of a strong dependence of image contrast on dose rate, which was recently discovered and is shown in Fig. 7b [31,32]. The result suggests that reliable contrast measurements require dose rates around one atto Ampere/Å^2, which are not yet applied in this study that uses medium dose rates.

In summary, we have studied the atomic structure and interfaces of Cu_2S and CdS/Cu_2S nancrystals at atomic resolution. After synthesis these nanorods exhibit a low-chalcocite structure ($P2_1/c$) that transforms into a high-chalcocite phase ($P6_3/mmc$) during electron irradiation. In the CdS/Cu_2S heterostructured nanorods the electron beam further stimulates ion exchange such that the Cu_2S phase moves into CdS phase, which requires copper in-diffusion and cadmium extraction to be solved in the solution, which is consistent with the growth process. The copper/cadmium exchange can be observed time resolved by tracking the positions of CdS/Cu_2S interfaces in phase images of exit wave functions that are reconstructed from subsets of one extended focus series. In recording conditions that allow for atomic resolution, a reduction of the electron beam current and voltage are most effective options to minimize beam–sample interactions and maintain pristine structures. A comparison of electron beam-induced interface migration caused by copper/cadmium exchange with available copper diffusion data from CdS/Cu_2S thin film solar cells yields an agreement within a factor of 3–10 for copper diffusion data from grain boundaries with an activation energy of 0.96 eV. A tendency is observed, which suggests that copper interdiffusion across interfaces in heterostructured nanocrystals is retarded if compared to the copper diffusion in polycrystalline thin film materials.

Acknowledgments

The TEM characterizations were performed at the National Center for Electron Microscopy, Lawrence Berkeley National Lab which is supported by the U.S. Department of Energy under Contract no. DE-AC02-05CH11231. HZ thanks the support of DOE Early Career Research Program.

References

[1] J.H.C. Hadley, W.F. Tseng, Journal of Crystal Growth 39 (1977) 61.
[2] S. Martinuzzi, Solar Cells 5 (1981) 243.
[3] R.D. Robinson, B. Sadtler, D.O. Demchenko, C.K. Erdonmez, L.W. Wang, A.P. Alivisatos, Science 317 (2007) 355.
[4] Y. Wu, C. Wadia, W. Ma, B. Sadtler, A.P. Alivisatos, Nano Letters 8 (2008) 2551.
[5] B. Sadtler, D.O. Demchenko, H. Zheng, S.M. Hughes, M.G. Merkle, U. Dahmen, L.W. Wang, A.P. Alivisatos, Journal of the American Chemical Society 131 (2009) 5285.
[6] J.L. Baker, A. Widmer-Cooper, M.F. Toney, P.L. Geissler, A.P. Alivisatos, Nano Letters 10 (2010) 195.
[7] J. Tang, Z. Huo, S. Brittman, H. Gao, P. Yang, Nature Nanotechnology 6 (2011) 568.
[8] A.C. Rastogi, S. Salkalachen, Solar Cells 9 (1983) 185.
[9] H.M. Zheng, J.B. Rivest, T.A. Miller, B. Sadtler, A. Lindenberg, M.F. Toney, L.W. Wang, C. Kisielowski, A.P. Alivisatos, Science 333 (2011) 206.
[10] C. Kisielowski, B. Freitag, M. Bischoff, H. van Lin, S. Lazar, G. Knippels, P. Tiemeijer, M. van der Stam, S. von Harrach, M. Stekelenburg, M. Haider, S. Uhlemann, H. Mueller, P. Hartel, B. Kabius, D. Miller, I. Petrov, E.A. Olson,

T. Donchev, E.A. Kenik, A.R. Lupini, J. Bentley, S.J. Pennycook, I.M. Anderson, A.M. Minor, A.K. Schmid, T. Duden, V. Radmilovic, Q.M. Ramasse, M. Watanabe, R. Erni, E.A. Stach, P. Denes, U. Dahmen, Microscopy and Microanalysis 14 (2008) 469.
[11] B. Barton, B. Jiang, C. Song, P. Specht, H. Calderon, C. Kisielowski, Microscopy and Microanalysis 18 (2012) 982.
[12] R.W. Potter, Economic Geology 72 (1977) 1524.
[13] H.T. Evans, Science 203 (1979) 356.
[14] H.T. Evans, Nature Physical Science 232 (1971) 69.
[15] J.B. Rivest, L.K. Fong, P.K. Jain, M.F. Toney, A.P. Alivisatos, Journal of Physical Chemistry Letters 2 (2011) 2402.
[16] P.C. Tiemeijer, M. Bischoff, B. Freitag, C. Kisielowski, Ultramicroscopy 118 (2012) 35.
[17] W.O. Saxton, Advances in Electronics and Electron Physics, Computer Techniques for Image Processing in Electron Microcopy, Academic Press, New York, 1978.
[18] W.O. Saxton, Journal of Electron Spectroscopy 5 (1980) 665.
[19] D. Van Dyck, M. Op De Beeck, Proceedings of the 12th International Congress for Electron Microscopy, Seattle, 1990, p. 26.
[20] M. Op De Beeck, D. Van Dyck, W. Coene, Ultramicroscopy 64 (1996) 167.
[21] D. Van Dyck, M. Op De Beeck, W. Coene, Optik 93 (1993) 103.
[22] S. Van Aert, P. Geuens, D. Van Dyck, C. Kisielowski, J.R. Jinschek, Electron channelling based crystallography, Ultramicroscopoy 107 (2007) 551.
[23] J.R. Jinschek, K. Batenburg, H.A. Calderon, R. Kilaas, V. Radmilovic, C. Kisielowski, Ultramicroscopy 108 (2008) 589.
[24] D. Van Dyck, J.R. Jinschek, F.-R. Chen, Nature 486 (2012) 243.
[25] W.-K. Hsieh, F.-R. Chen, J.-J. Kai, A.I. Kirkland, Ultramicroscopy 98 (2004) 99.
[26] ⟨http://www.totalresolution.com/⟩.
[27] R. Brydson, Electron Energy Loss Spectroscopy, BIOS, Oxford, 2001.
[28] L. Manna, E.C. Scher, A.P. Alivisatos, Journal of the American Chemical Society 122 (2000) 12700.
[29] Z.A. Peng, X. Peng, Journal of the American Chemical Society 123 (2001) 1389.
[30] G. Bertoni, V. Grillo, R. Brescia, X. Ke, S. Bals, A. Catellani, H. Li, L. Mann, ACS Nano 6 (2012) 6453.
[31] P. Specht, R.J. Gulotty, D. Barton, R. Cieslinski, S. Rozeveld, J.H. Kang, O. Dubon, ChemCatChem 3 (2011) 1034–1037.
[32] C. Kisielowski, L.-W. Wang, P. Specht, H.A. Calderon, B. Barton, B. Jiang, J.H. Kang, R. Cieslinski, 2013 (in review).